# Piezobirefringence above the fundamental edge in Si

Meera Chandrasekhar, M. H. Grimsditch, and M. Cardona
*Max-Planck-Institut für Festkörperforschung, 7 Stuttgart 80, Federal Republic of Germany*
(Received 21 February 1978)

We report measurements of stress-induced birefringence in silicon in a spectral region (1.65 to 3.4 eV) where the material is opaque. A new technique that employs Raman scattering is used to extend the range of previous measurements performed in the transparent region below 1.2 eV. Theoretical fits to the data are made by considering the contributions to piezobirefringence due to the $E_1$, $E_1+\Delta_1$, and $E_2$ transitions under uniaxial stresses along the [001] and [111] directions.

## I. INTRODUCTION

Stress-induced birefringence in cubic semiconductors that are optically isotropic if unstressed has been studied in a variety of materials[1,2] near and below the fundamental edge. Conventional techniques[1-3] employ transmission of light through the sample, and are consequently limited to a frequency region where the material is transparent. In the opaque region above the fundamental edge limited success has been reported in obtaining relative values of the piezo-optical constants in silicon using data obtained from piezoreflectance.[4,5] These difficulties have been overcome with a new technique that employs Raman scattering[6]: using this method we have already reported[6] measurements of the magnitudes of the piezo-optical constants $\pi_{11}-\pi_{12}$ and $\pi_{44}$ at 1.92 eV, well above the fundamental gap of 1.1 eV. In this paper we present measurements of the piezo-optical constants in the energy range from 1.65 to 3.4 eV, a region easily accessible to conventional lasers.

Previous measurements[1] of piezobirefringence in silicon in the transparent region between 0.6 and 1.2 eV exhibit little dispersion near the fundamental edge. This is a consequence of the indirect nature of the fundamental edge in this material, which is too weak to contribute significantly to the real part of the dielectric constant. The present measurements approach the direct gap in Si (~3.3 eV) and show a strong dispersion near this gap similar to the results obtained for the direct gaps of Ge and GaAs.[1] We calculate the contribution to the piezobirefringence due to the $E_1$, $E_1+\Delta_1$ gaps, which provide the main dispersive terms around 3.3 eV, while the $E_2$ gap at 4.4 eV contributes only a slowly varying term in the region of interest. The contribution from the $E_0'$ gap, also near 3.3 eV, is neglected owing to its small oscillator strength. The calculations are compared with experiment, and good agreement is obtained using the deformation potentials of the $E_1$, $E_1+\Delta_1$ transitions and the magnitude of the contribution from the $E_2$ gap as adjustable parameters. The deformation potentials used agree with previous measurements of these quantities to within a factor of 2, which may be a result of the simple model we have used to fit the experimental data.

Pure Si (carrier concentration $10^{13}$ cm$^{-3}$) was used in our experiments in order to eliminate any free-carrier effects. All experiments were performed at room temperature. Uniaxial stress was applied along the [100] and [110] directions to determine $\pi_{11}-\pi_{12}$ and $\pi_{44}$, respectively.

The experimental details are described in Sec. II; Section III presents the experimental results and their analysis, while Sec. IV provides a discussion and theoretical interpretation of the experimental results. Section V reviews the main conclusions of the work.

## II. EXPERIMENTAL DETAILS

Raman measurements were performed in the back-scattering geometry standard for opaque materials. $Ar^+$ and $Kr^+$ lasers were used to obtain the exciting radiation, the polarization of which was turned with a polarization rotator to obtain light linearly polarized at 45° to the stress axis. The scattered light was analyzed with a sheet polarizer. Standard polarization rotators and analysers could not be used in the ultraviolet at 3638 Å; therefore, a combination of a 3600-Å quarter-wave plate and a Babinet compensator were used to rotate the polarization of the incident light, and a Glan Thomson prism was used as an analyzer. The detection system consisted of a double monochromator with holographic gratings, a cooled photomultiplier equipped with photon-counting electronics, and a multichannel analyzer for data storage. The stress apparatus equipped with digital readout has been described previously in the literature.[7] Compressive stresses up to a maximum of 22 kbar were applied to the samples that had a typical cross section of

 

$1.3 \times 1.3$ mm$^2$. The samples were cut and x-ray oriented to within 1°, and the face used for scattering was polished with 0.3-$\mu$m alumina and polish etched with Syton[8] for 10 min.

### III. EXPERIMENTAL RESULTS AND ANALYSIS

When a uniaxial stress is applied to a cubic crystal, the crystal becomes birefringent, and a phase difference is induced between the components of light polarized parallel and perpendicular to the stress axis. This stress-induced birefringence causes a depolarization of the incident and scattered radiation within the crystal in a manner similar to that observed in light-scattering experiments in birefringent materials.[9] This depolarization is used to measure the stress-induced birefringence coefficients (piezo-optical constants). The method[6] is as follows: Raman scattering is observed in a back-scattering geometry standard for opaque materials. A Raman-active structure and a sample orientation are chosen such that in a configuration with light polarized and analyzed at 45° to the stress direction, the structure under consideration (a phonon or an overtone) has zero Raman intensity at zero stress. When a stress is applied, the intensity increases from zero due to the stress-induced birefringence which changes the polarization of the incident and scattered fields within the crystal. Likewise the same phonon or overtone in a different polarization configuration (also at 45° to the stress direction) that has maximum Raman intensity at zero stress, decreases in intensity on the application of stress. The ratio of the two intensities as a function of stress is used to determine the absolute values of the piezo-optical constants $\pi_{11} - \pi_{12}$ and $\pi_{44}$. No information is obtained on the hydrostatic piezo-optical constant $\pi_{11} + 2\pi_{12}$ since the birefringence is induced by the shear component of the stress.

Details of the theoretical analysis have been published elsewhere.[6] A brief description follows. To describe the scattering geometry, a coordinate system is chosen such that the $\hat{z}$ axis is perpendicular to the scattering face. The stress direction is chosen to be $(1/\sqrt{2})(\hat{x}+\hat{y})$, while $(1/\sqrt{2})(\hat{x}-\hat{y})$ is perpendicular to both $\hat{z}$ and the stress direction. The stress is chosen along either [100] or [110] crystal directions, $\hat{z}$ being along either [001] or [1$\bar{1}$0] for each stress direction. On the application of stress, a phase difference $\phi$ is induced between the electric vectors of the radiation polarized parallel and perpendicular to the stress, for both the incident and scattered light.

For incident or scattered polarizations of light along $\hat{x}$ or $\hat{y}$ (at 45° to the stress axis) the electric vectors will be

$$\begin{aligned} \hat{e}_x &= \tfrac{1}{2}[(\hat{x}+\hat{y}) + (\hat{x}-\hat{y})e^{i\phi}], \\ \hat{e}_y &= \tfrac{1}{2}[(\hat{x}+\hat{y}) - (\hat{x}-\hat{y})e^{i\phi}], \end{aligned} \tag{1}$$

respectively, where $\phi$ is the phase difference at a depth $l$ within the crystal, and is given by

$$\phi(2\pi/\lambda)(n_{\parallel} - n_{\perp})l, \tag{2}$$

where $n_{\parallel}$ and $n_{\perp}$ are the refractive indices for light polarized parallel and perpendicular to the stress direction; the difference $n_{\parallel} - n_{\perp}$ is linear in stress and depends on the sample orientation. $\lambda$ is the wavelength of the incident or scattered radiation, which are taken to be equal owing to the small frequency of the phonon as compared with that of the incident or scattered radiation.

At a depth $l$ within the crystal, the intensity of the incident light is attenuated by a factor $e^{-\alpha_i l}$, where $\alpha_i$ is the absorption coefficient at the incident frequency. The scattered light is similarly attenuated with an absorption coefficient $\alpha_s$. Using the electric vectors in Eq. (1) and the Raman tensor $R_j$ of the phonon ($j$ labels degenerate phonons) the total intensity due to a phonon observed in a given polarization configuration, say $z(xx)\bar{z}$, can be calculated to be

$$I_{xx} = \int_0^{\infty} \sum_j |\hat{e}_x \cdot R_j \cdot \hat{e}_x|^2 e^{-(\alpha_i + \alpha_s)l}\, dl \tag{3a}$$

and similarly for the $z(xy)\bar{z}$ configuration

$$I_{xy} = \int_0^{\infty} \sum_j |\hat{e}_x \cdot R_j \cdot \hat{e}_y|^2 e^{-(\alpha_i + \alpha_s)l}\, dl\,, \tag{3b}$$

where factors common to Eqs. (3a) and (3b) have been dropped. The standard notation for scattering geometries is used, i.e., $z(xy)\bar{z}$ denotes that the incident and scattered wave vectors are along $z$ and $\bar{z}$, while $x$ and $y$ denote the polarizations of the incident and scattered radiation, respectively.

The scattering face and stress direction are chosen such that one of the intensities $I_{xx}$ or $I_{xy}$ for the chosen phonon is zero and the other nonzero at zero stress. The intensity ratio $\beta = I_{xx}/I_{xy}$ or $I_{xy}/I_{xx}$ is defined so that $\beta = 0$ at zero stress, and is obtained from Eqs. (3) as a function of stress. For a given sample orientation $\beta$ is related through $n_{\parallel} - n_{\perp}$ to the piezo-optical constants. Several combinations of phonons and sample orientations can be used to determine the magnitude (not the sign) of $\pi_{11} - \pi_{12}$ and $\pi_{44}$. Six possible combinations are summarized in Table I. In each case we list the stress direction (column 1), scattering face (column 2), the electric vectors $\hat{e}_x$ and $\hat{e}_y$ in terms of the crystallographic directions (column 3), the intensities of the $\Gamma_1$ and $\Gamma_{25'}$ components of the Raman tensor seen in the $(xx)$

TABLE I. Six configurations for measuring the piezo-optical constants.

| Case | (1) Stress direction | (2) Scattering-face $\hat{z}$ | (3) Electric vectors of incident and scattered radiation $\hat{e}_x$ | $\hat{e}_y$ | (4) Components of the Raman tensor in the $z(xx)\bar{z}$ and $z(xy)\bar{z}$ configurations [a] | (5) Phonon chosen and its symmetry | (6) Intensity ratio $\beta$ given by | (7) Piezo-optical coefficient measured |
|---|---|---|---|---|---|---|---|---|
| (a) | [110] | [001] | [100] | [010] | $\Gamma_1$<br>$\Gamma_{25'}$ | O(Γ), $\Gamma_{25'}$ | Eq. (4) | $\pi_{44}$ |
| (b) | [001] | [100] | [110] | [1$\bar{1}$0] | $\Gamma_1+\Gamma_{25'}$<br>0 | 2 TA($X$), $\Gamma_1$ | Eq. (5) | $\pi_{11}-\pi_{12}$ |
| (c) | [111] | [1$\bar{1}$0] | [001] | [110] | $\Gamma_1$<br>$\Gamma_{25'}$ | O(Γ), $\Gamma_{25'}$ | Eq. (7) | $\pi_{44}$ |
| (d) | [110] | [001] | [100] | [010] | $\Gamma_1$<br>$\Gamma_{25'}$ | 2 TA($X$), $\Gamma_1$ | Eq. (8) | $\pi_{44}$ |
| (e) | [001] | [100] | [110] | [1$\bar{1}$0] | $\Gamma_1+\Gamma_{25'}$<br>0 | O(Γ), $\Gamma_{25'}$ | Eq. (9) | ··· |
| (f) | [110] | [1$\bar{1}$0] | [11$\sqrt{2}$] | [11$\sqrt{\bar{2}}$] | $\Gamma_1+\frac{5}{4}\Gamma_{25'}$<br>$\frac{1}{4}\Gamma_{25'}$ | 2 TA($X$), $\Gamma_1$ | Eq. (10) | $\frac{1}{2}(\pi_{11}-\pi_{12}+\pi_{44})$ |

[a] The $\Gamma_{12}$ component has been omitted since both the O(Γ) and 2 TA($X$) phonons have negligible intensity in this component.

and $(xy)$ polarization configurations at zero stress (column 4), the phonon chosen and its symmetry [the zone-center phonon O(Γ) has $\Gamma_{25'}$ symmetry, while the second-order acoustic phonon 2TA($X$) has mainly $\Gamma_1$ symmetry] (column 5), the intensity ratio $\beta$ for the chosen phonon as a function of stress (column 6), and the piezo-optical constant measured in that configuration (column 7). The direction of applied stress and the face used determines which piezo-optical constant is measured,[10] independent of the phonon used. The functional form of $\beta$, however, is dependent on both the sample orientation and the phonon symmetry. Of the six cases listed in Table I, we chose two simple cases (a) and (b) to measure $\pi_{11}-\pi_{12}$ and $\pi_{44}$ as a function of incident frequency. The four others were used as confirming checks.

Careful alignment of the polarizer and analyzer at zero stress was necessary in order to obtain the best extinction ratio between the nonallowed and allowed configurations for the chosen phonon. Although one expects $\beta=0$ at zero stress, small misalignments of the sample and possible leakage through the polarization rotator and analyzer are believed to be the main cause of the small intensity seen in a forbidden configuration at zero stress. This leakage was observed to increase with increasing exciting energy, varying after the background was subtracted, from 1% at 1.65 eV to 5% at 3.4 eV for the zone-center phonon, with similar numbers for 2TA($X$) scattering. Part of this leakage is, of course, due to the finite angle of incidence ($\lesssim 30°$) used in the experiments, which in itself rotates the direction of polarization in the unstressed crystal by ~2°. We corrected for this effect by slightly rotating the polarizer and analyzer to make sure that we were at the maximum or minimum of scattered intensity, as required. The increase in "leakage" with increasing photon energy mentioned above may be due to the increasing extinction coefficient which results, for non-normal incidence, in elliptically polarized light inside the unstressed sample and thus makes extinction by readjusting polarizers impossible.

*Case (a).* Stress $\vec{X} \parallel [110]$, scattering from a (001) face produced by the zone-center optical phonon O(Γ) of $\Gamma_{25'}$ ($T_{2g}$) symmetry at a frequency of 520 cm$^{-1}$. It has zero intensity in the $z(xx)\bar{z}$, and a maximum intensity in the $z(xy)\bar{z}$ configuration at zero stress where $\hat{x}$ is [100] and $\hat{y}$ is [010] (Table I).

The intensity ratio is therefore defined as $\beta = I_{xx}/I_{xy}$, which is zero at zero stress. Upon the application of stress, the intensity of the zone-center phonon in the $(xx)$ configuration grows at the expense of that in the $(xy)$ configuration. In Fig. 1 we plot the data obtained for the zone-center phonon in the $(xx)$ and $(xy)$ configurations at zero and 20 kbar for an exciting wavelength of 7525 Å. The intensity of the $(xx)$ mode is 1%

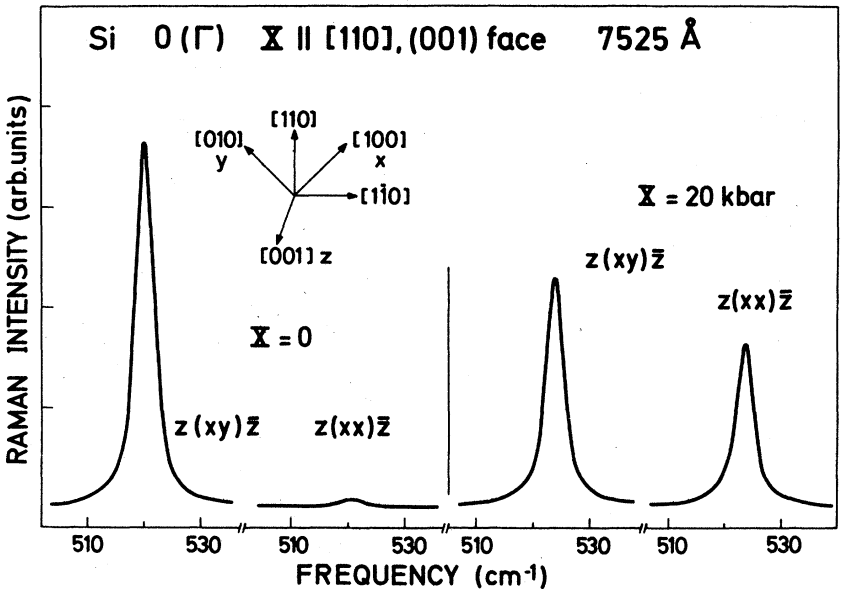


FIG. 1. Birefringence-induced changes in the intensity of the optical phonon for stress $\vec{X} \| [110]$, measured with an exciting wavelength of 7525 Å. The intensity ratio $\beta$ grows from 1% at zero stress to about 70% at 20 kbar.

that of the $(xy)$ mode at zero stress, and the ratio grows to about 70% at 20 kbar. The calculated intensity ratio as a function of stress, obtained by substituting the appropriate Raman tensor[11] and integrating Eq. (3), is

$$\beta = \frac{I_{xx}}{I_{xy}} = \frac{1}{1 + 1/2(AX)^2} , \tag{4a}$$

where $X$ is the applied stress and

$$A = \pi n_0^3 \pi_{44} / \lambda (\alpha_i + \alpha_s) \tag{4b}$$

is obtained by substituting the relation for $n_{\|} - n_{\perp}$ for this sample orientation[10] in Eq. (2),

$$n_{\|} - n_{\perp} = -\tfrac{1}{2} n_0^3 \pi_{44} X , \tag{4c}$$

where $X$ is negative for the compressive stresses used in our experiments, and $n_0$ is the refractive index at zero stress.

In Fig. 2 we plot the intensity ratio $\beta$ versus stress $X$ for several exciting wavelengths. The solid lines are fits to experimental data using Eq. (4a). The best fits were achieved by shifting the zero on the $\beta$ axis by a small constant to take care of the leakage at zero stress. We note in Fig. 2 that the variation of $\beta$ with stress depends strongly on the exciting frequency. The largest change in $\beta$ with stress occurs at the longest wavelength, 7525 Å, where the penetration depth $[\frac{1}{2}(\alpha_i + \alpha_s)]^{-1}$ is the largest (approximately $7 \times 10^4$ Å), while the smallest change is observed at 3638 Å, where the penetration depth is about 125 Å. From the best fits to the data we obtain the parameter $A$ and hence the magnitude of $\pi_{44}$ for each wavelength. The values found are listed in Table II.

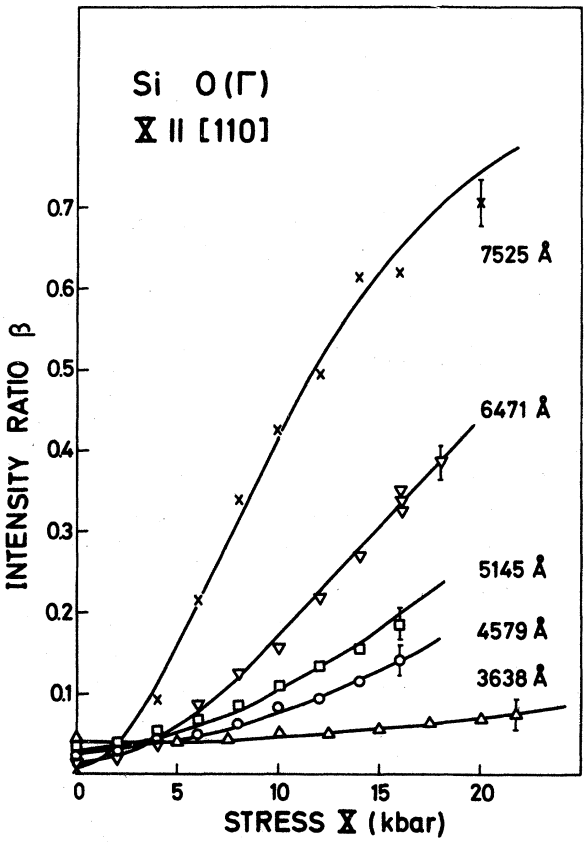


FIG. 2. Intensity ratio $\beta$ vs stress $X$ for the zone-center optical phonon under [110] stress [case (a)]. The experimental results for five different exciting wavelengths (marked in the figure) are fit using Eq. (4). The best fits obtained are indicated by the solid lines.

TABLE II. Magnitudes of the piezo-optical constants obtained for different exciting frequencies. The signs of $\pi_{11}-\pi_{12}$ and $\pi_{44}$ can be inferred to be negative from comparison with long-wavelength data from Ref. 1. The superscripts a–f refer to the various scattering geometries given in Table I.

| Exciting wavelength (Å) | $\pi_{11}-\pi_{12}$ ($10^{-14}$ cm$^2$/dyn) | $\pi_{44}$ ($10^{-14}$ cm$^2$/dyn) | $\frac{1}{2}(\pi_{11}-\pi_{12}+\pi_{44})$ ($10^{-14}$ cm$^2$/dyn) |
|---|---|---|---|
| 3638 | | 32.3 ±5.5 [a] | |
| 4579 | 5.9 ±0.7 [b] | 10.5 ±0.7 [a] | |
| 5145 | 8.1 ±0.7 [b] | 8.6 ±0.5 [a] | |
| 6471 | 9.3 ±0.6 [b] | 6.9 ±0.5 [a] | 8.8 ±0.5 [f] |
| | | 7.5 ±0.5 [c] | |
| | | 7.7 ±0.5 [d] | |
| 7525 | | 7.25 ±0.3 [a] | |

*Case (b).* Stress $\vec{X}\|[001]$, (100) face: The second-order acoustical phonon 2TA($X$) at a frequency of approximately 300 cm$^{-1}$ has mainly $\Gamma_1$ ($A_{1g}$) symmetry. It has zero intensity (Table I) in the $z(xy)\bar{z}$ configuration and a nonzero intensity in the $z(xx)\bar{z}$ configuration, where $x$ and $y$ are defined in Table I. Hence $\beta = I_{xy}/I_{xx}$, and the stress dependence is given by

$$\beta = \frac{I_{xy}}{I_{xx}} = \frac{1}{1+1/2(BX)^2}\ , \tag{5a}$$

where

$$B = \pi n_0^3(\pi_{11}-\pi_{12})/\lambda(\alpha_i+\alpha_s)\,. \tag{5b}$$

The piezo-optical coefficient $\pi_{11}-\pi_{12}$ obtained in this configuration is related to $n_\parallel - n_\perp$ through[10]

$$n_\parallel - n_\perp = -\tfrac{1}{2}n_0^3(\pi_{11}-\pi_{12})X. \tag{5c}$$

The same functional form for $\beta$ is found as for the optical phonon in case (a); in Fig. 3 we plot $\beta$ vs $X$ in this configuration for different exciting frequencies. The solid lines are fits to the experimental points using Eq. (5a). The uncertainties in these fits are somewhat larger than for the O($\Gamma$) optical phonon since the 2TA($X$) mode is weaker than the optical phonon. The intensities $I_{xx}$ and $I_{xy}$ were obtained by tuning the monochromator to the peak of the 2TA($X$) structure and counting the number of scattered photons in a 5-min interval. Contrary to the case of the O($\Gamma$) optical phonon, it was not necessary to scan the monochromator or to retune it after stress was applied because of the small shift of the 2TA($X$) structure with stress (approximately 0.15 cm$^{-1}$/kbar of uniaxial stress[12]) as compared with its large linewidth. Since good resolution was not required, wide slits were used to eliminate any errors introduced by not scanning the monochromater. Values of $\pi_{11}-\pi_{12}$ obtained in this configuration are listed in Table II. Two of the wavelengths used for the optical phonon, 7525 and 3638 Å, could not be conveniently used for the 2TA($X$) owing to the lower available laser power (150 mW as against 500 mW for the 4579, 5145, and 6471 Å lines) and consequent low signal for 2TA($X$) scattering.

The two cases discussed above are sufficient to obtain $\pi_{11}-\pi_{12}$ and $\pi_{44}$. The following four cases were measured for a single wavelength (6471 Å) in order to check the self-consistency of the analysis of the experimental data.

*Case (c).* Stress $\vec{X}\|[111]$, $(1\bar{1}0)$ face. The zone-

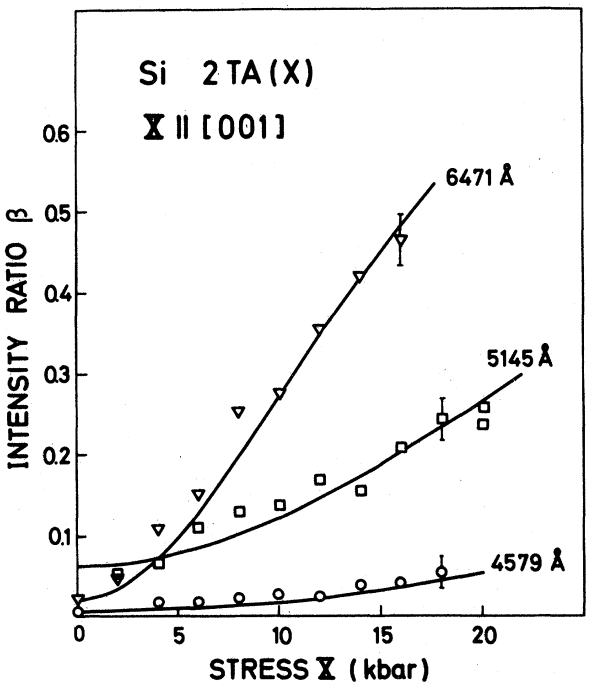


FIG. 3. Intensity ratio $\beta$ vs stress $X$ for the second-order acoustical phonon 2TA($X$) under [100] unaxial stress. The experimental data for three exciting wavelengths are fit using Eq. (5) (solid lines).

center optical phonon has zero intensity in the $z(x'x')\bar{z}$ configuration and a nonzero intensity in the $z(x'y')\bar{z}$ configuration (Table I), where $x'$ is [001] and $y'$ is [110].

The electric vectors given in Eq. (1) are easily rewritten to account for the fact that the polarizations are not at 45° to the stress: since the $[11\bar{2}]$ direction is at 90° to both the normal to the scattering face and the stress direction,

$$\hat{e}_{x'}=\frac{1}{3}([111]-[11\bar{2}]e^{i\phi}),$$
$$\hat{e}_{y'}=\frac{1}{3\sqrt{2}}(2[111]+[11\bar{2}]e^{i\phi}). \tag{6}$$

$I_{x'x'}$ and $I_{x'y'}$ are defined in a manner similar to Eq. (3). $\beta$ is obtained to be

$$\beta=\frac{I_{x'x'}}{I_{x'y'}}=\frac{16(AX)^2[1+2(AX)^2]}{9+33(AX)^2+20(AX)^4} \tag{7}$$

and $A$ is defined in Eq. (4b). In Fig. (4a) we plot $\beta$ vs $X$ in this configuration for an exciting wavelength of 6471 Å. The fit (solid line) to Eq. (7) gives the parameter $A$ and therefore $\pi_{44}$, which is found, within experimental error, to be the same as that obtained in case (a) (Table II).

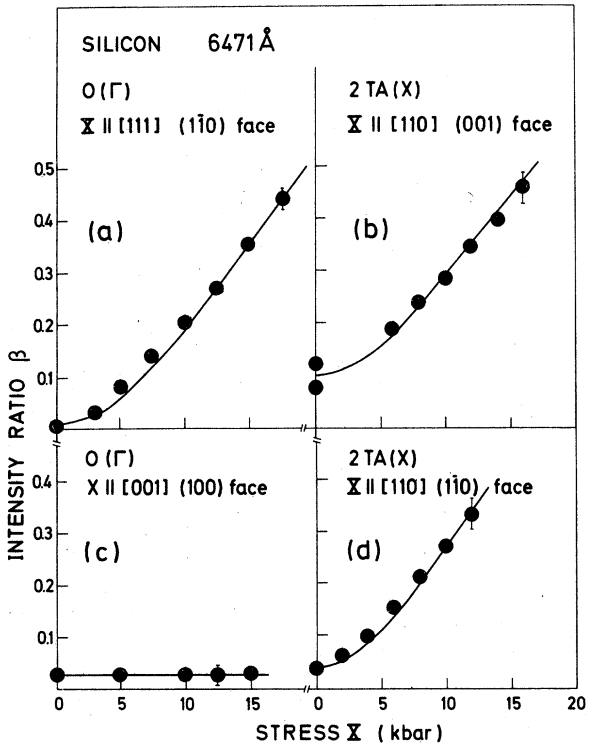


FIG. 4. Intensity ratios $\beta$ vs stress $X$ for an exciting wavelength of 6471 Å. The filled circles are experimental points. The solid lines are fits using the appropriate expressions given in the text: (a) represents case (c), (b) represents case (d), (c) represents case (e), and (d) represents case (f) (Table I).

*Case (d).* Stress $\vec{X}\parallel[110]$, (001) face: the second order acoustical phonon 2TA($X$) was used to obtain $\pi_{44}$ in a manner similar to case (a). $\beta=I_{xy}/I_{xx}$ and is given as a function of stress by

$$\beta=\frac{I_{xy}}{I_{xx}}=\frac{1}{1+1/2(AX)^2}, \tag{8}$$

a functional form identical to Eq. (4a) in case (a).

The experimental data obtained and the fit to Eq. (8) are shown in Fig. (4b). The value of $\beta$ at zero stress is seen to be quite large ($\simeq$10%) in this configuration. This is explained by the fact that a small component ($\simeq$5%–10%) of the intensity of the 2TA($X$) scattering appears in $\Gamma_{25'}$, symmetry,[13] while the rest appears in $\Gamma_1$ symmetry. At zero stress the component of $\Gamma_{25'}$ symmetry is allowed in the ($xy$) configuration, while that of $\Gamma_1$ symmetry appears in the ($xx$) configuration (Table I) so that at zero stress $\beta$ is not zero but the ratio of the intensities of the $\Gamma_{25'}$ and $\Gamma_1$ components of the 2TA($X$) (plus the leakage). Since the $\Gamma_{25'}$ component of the 2TA($X$) is small, we neglect any changes due to stress, and fit the experimental data with Eq. (8) by shifting the zero on the $\beta$ axis as in the other cases. The value of $\pi_{44}$ obtained is in agreement with cases (a) and (c) within experimental error (Table II).

*Case (e).* Stress $\vec{X}\parallel[001]$, (100) face. The optical phonon O($\Gamma$) is observed (Table I) in the $z(xx)\bar{z}$ configuration but not in the $z(xy)\bar{z}$ configuration. Equations (3) yield for this case

$$\beta=\frac{I_{xy}}{I_{xx}}=0 \tag{9}$$

as a function of stress. The experimental intensity ratio shown in Fig. (4c) also remains unchanged under stress and is equal to the leakage at zero stress. This configuration provides a useful check on our theoretical analysis of intensity ratios.

Case (f). Stress $\vec{X}\parallel[110]$, (1$\bar{1}$0) face. The major ($\Gamma_1$) component of the 2TA($X$) scattering has nonzero intensity in the $z(xx)\bar{z}$ configuration and zero intensity in the $z(xy)\bar{z}$ configuration (Table I). $\beta$ as a function of stress is

$$\beta=\frac{I_{xy}}{I_{xx}}=\frac{1}{1+1/2(CX)^2}, \tag{10a}$$

where

$$C=\pi n_0^3(\pi_{11}-\pi_{12}+\pi_{44})/2\lambda(\alpha_i+\alpha_s). \tag{10b}$$

Figure 4(d) shows experimental data and the fit to Eq. (10a), from which we obtain $\frac{1}{2}(\pi_{11}-\pi_{12}+\pi_{44})$. The result agrees with values obtained for $\pi_{11}-\pi_{12}$ and $\pi_{44}$ using cases (a)–(d) for the same exciting wavelength of 6471 Å (Table II). We note

again that the experiments yield only the absolute value of the corresponding piezo-optical coefficients. Their sign must be determined by extrapolation to long wavelengths and comparison with the sign obtained in the classical stress-induced birefringence measurements performed in the region of transparency.[1] Equation (10b), however, enables us to determine the relative sign of $\pi_{11} - \pi_{12}$ and $\pi_{44}$ once their magnitudes have been found from the other experimental configurations: they are found to have the same sign (Table II), in agreement with the negative signs found for both piezo-optical constants at long wavelengths[1] (Sec. IV).

The values of $\pi_{11} - \pi_{12}$ and $\pi_{44}$ obtained from these experiments are summarized in Table II. A wide spectrum of available laser lines, from 7525 to 3638 Å, were used. The values of the average refractive index $n_0$ and the absorption coefficient $\frac{1}{2}(\alpha_i + \alpha_s)$ (averaged between incident and scattered frequencies for both 2TA($X$) and O($\Gamma$) phonons[14]) are listed in Table III. In Fig. 5 we plot the values obtained for the piezo-optical constants $\pi_{11} - \pi_{12}$ (triangles) and $\pi_{44}$ (circles) as a function of energy. In the figure we include the piezo-optical constants obtained from the data of Higginbotham *et al.*[1] in the energy region below 1.2 eV. The solid lines are theoretical fits to be discussed in Sec. IV.

In calculating the contribution to the stress-induced birefringence from microscopic theory, one obtains directly the difference between the dielectric constants parallel and perpendicular to the stress direction $\epsilon_{\parallel} - \epsilon_{\perp}$, which is related to the quantity $n_{\parallel} - n_{\perp}$ in Eq. (2) through the standard relation

$$\epsilon = n^2 . \tag{11a}$$

We neglect the imaginary parts of the dielectric constant and the refractive index, which should be a fairly good approximation below the $E_0'$ and $E_1$, $E_1 + \Delta_1$ gaps (below 3.3 eV). Then

$$\epsilon_{\parallel} - \epsilon_{\perp} = 2n_0(n_{\parallel} - n_{\perp}) . \tag{11b}$$

A piezo-optical constant, for example $\pi_{44}$, is then related to $\epsilon_{\parallel} - \epsilon_{\perp}$ by [Eq. (4c)]

$$\pi_{44} = -\frac{1}{n_0^4}\left(\frac{\epsilon_{\parallel} - \epsilon_{\perp}}{X}\right)_{\vec{X}\parallel[111]} \tag{11c}$$

$\pi_{11} - \pi_{12}$ is related in a similar manner to $(\epsilon_{\parallel} - \epsilon_{\perp})/X$ for a stress parallel to [001].

In order to directly compare experiment with theory we plot in Fig. 6 the experimental values of $(\epsilon_{\parallel} - \epsilon_{\perp})/X$ for stress $\vec{X} \parallel [001]$ (triangles) obtained from our data in case (b) (Fig. 3) and from Ref. 1 for the energy range from 0.6 to 1.2 eV. For stress $\vec{X} \parallel [110]$ $(\epsilon_{\parallel} - \epsilon_{\perp})/X$ is plotted in Fig. 7 (circles) using data from case (a) (Fig. 2) and the data between 0.6 and 1.2 eV for stress $\vec{X} \parallel [111]$ in Ref. 1. (The piezo-optical coefficient obtained is $\pi_{44}$ in both cases.) The solid lines in Figs. 6 and 7 are theoretical fits and the squares are scaled values from piezoreflectance data; both will be discussed in Sec. IV.

## IV. THEORY AND DISCUSSION

The band structure of silicon is well known from a variety of calculations and experiments.[15-17]

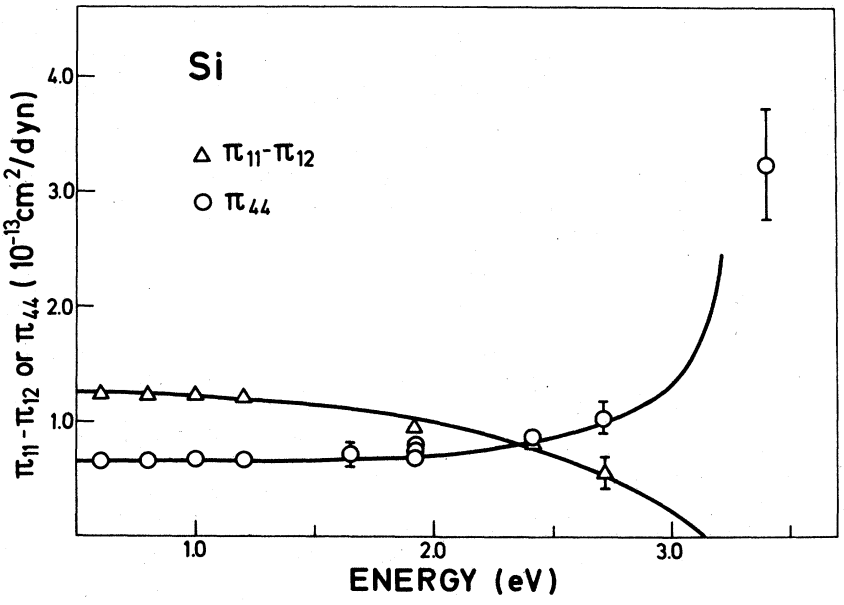


FIG. 5. Experimentally obtained values of the piezo-optical constants $\pi_{11} - \pi_{12}$ (triangles) and $\pi_{44}$ (circles) as a function of energy. The data below 1.5 are obtained from Ref. 1 and those above 1.5 eV from present investigations. The solid lines are theoretically calculated values obtained from the best fits to $(\epsilon_{\parallel} - \epsilon_{\perp})/X$ in Figs. 6 and 7.

TABLE III. Values of the refractive index $n_0$ and absorption coefficient $\frac{1}{2}(\alpha_i + \alpha_s)$ (averaged between incident and scattered frequencies) used for the optical phonon and the second-order acoustical phonon in calculating $\pi_{11} - \pi_{12}$ and $\pi_{44}$ (from Ref. 14).

| Exciting wavelength (Å) | O(Γ) $n_0$ | O(Γ) $\frac{1}{2}(\alpha_i + \alpha_s)$ ($cm^{-1}$) | 2 TA(X) $n_0$ | 2 TA(X) $\frac{1}{2}(\alpha_i + \alpha_s)$ ($cm^{-1}$) |
|---|---|---|---|---|
| 3638 | 6.75 | $6.36\times10^5$ | | |
| 4579 | 4.51 | $2.14\times10^4$ | 4.53 | $2.21\times10^4$ |
| 5145 | 4.17 | $9.75\times10^3$ | 4.18 | $1.0\times10^4$ |
| 6471 | 3.83 | $3.01\times10^3$ | 3.82 | $3.09\times10^3$ |
| 7525 | 3.70 | $1.28\times10^3$ | | |

The lowest direct transitions occur at an energy of about 3.3 eV. The major contribution to the dielectric constant arises from the $E_1$, $E_1+\Delta_1$ transitions along the ⟨111⟩ directions, and a contribution with low oscillator strength $E_0'$ arises from transitions at the center of the Brillouin zone. The next direct gap $E_2$ is at approximately 4.4 eV. Not many details are known about this gap; the corresponding transitions are believed to spread over a large region around the $X$ point in the Brillouin zone. We calculate contributions to piezobirefringence from the $E_1$, $E_1+\Delta_1$ and $E_2$ transitions, neglecting the $E_0'$ gap due to its low oscillator strength. The $E_1$, $E_1+\Delta_1$ transitions provide a strong dispersive term close to 3.3 eV, while the $E_2$ gap provides a background term in the energy region studied in our experiments (1.65–3.4 eV).

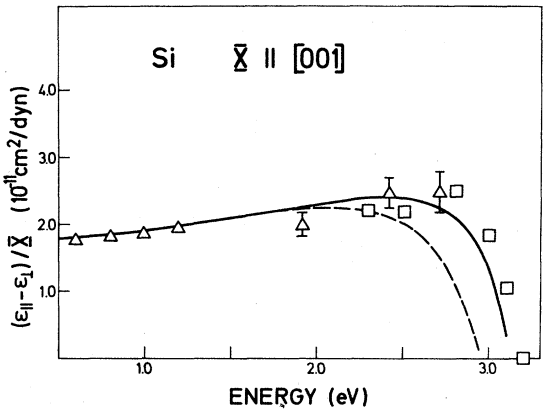


FIG. 6. $(\epsilon_{\parallel} - \epsilon_{\perp})/X$ as a function of energy for stress along [001]. The experimental data (triangles) were obtained from Ref. 1 (below 1.5 eV) and present measurements (above 1.5 eV). The solid line is the best fit using Eq. (20), obtained with $D_3^3 = -1.8$ eV and $C_2 = 2.27\times10^{-11}$ $cm^2$/dyn. The dashed line, which coincides with the solid line at low energies is obtained for $D_3^3 = -4$ eV and $C_2 = 2.8\times10^{11}$ $cm^2$/dyn. The squares are scaled values obtained from Ref. 7.

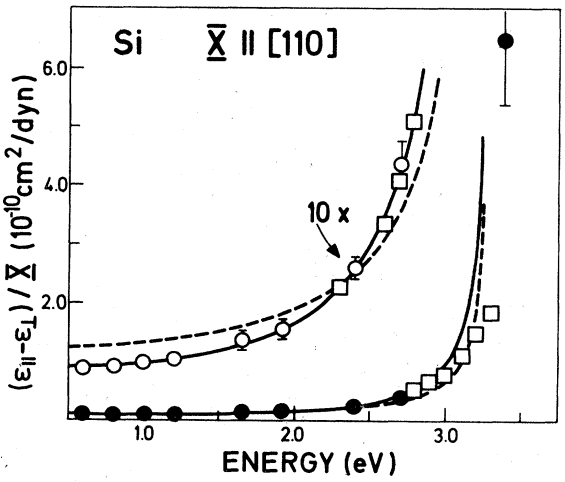


FIG. 7. $(\epsilon_{\parallel} - \epsilon_{\perp})/X$ as a function of energy for stress along [110]. The experimental data (circles) were obtained from Ref. 1 (below 1.5 eV) and present experiments (above 1.5 eV). The filled circles are plotted on the scale indicated in the figure, while the open circles are replots of the same values on an expanded (10×) scale. The squares are scaled values obtained from Ref. 5. The solid lines are the fits using Eq. (21), corresponding to $D_1^5 + 2\sqrt{2}D_3^5 = 40.6$ eV and $C_2' = -1.3\times10^{-11}$ $cm^2$/dyn. The dashed lines are obtained for $D_1^5 + 2\sqrt{2}D_3^5 = 22.3$ eV and $C_2' = 0$.

### A. Contribution from the $E_1$, $E_1+\Delta_1$ gaps

The $E_1$, $E_1+\Delta_1$ transitions arise from critical points along all the equivalent ⟨111⟩ directions.[18] The contribution to the real part of the dielectric constant from the $E_1$ critical points can be written as[1,19]

$$\epsilon_1(\omega) - 1 = \frac{-B}{\pi}|\langle|p|\rangle|^2 \frac{1}{\omega_1^2}\left(\frac{1}{x_1^2}\ln(1-x_1^2)\right), \quad (12a)$$

where

$$B = \frac{4\sqrt{3}\,\pi m^*}{a_0} \quad (12b)$$

(in atomic units). In Eq. (12b) $m^*$ is the effective mass perpendicular to the [111] direction and $a_0$ the lattice constant, $|\langle|p|\rangle|^2$ is the square of the transition matrix element between valence and conduction bands, $\omega_1$ the energy of the $E_1$ transition, and $x_1 = \omega/\omega_1$. A similar expression can be written for the $E_1+\Delta_1$ transition substituting $\omega_{1s} = \omega_1 + \Delta_1$ for $\omega_1$ and $x_{1s} = \omega/\omega_{1s}$ for $x_1$.

The birefringence induced in the material upon

the application of a uniaxial stress is discussed in Ref. 19. Two types of contributions have to be considered: those arising from stress induced changes in matrix elements and those due to the splitting of the various equivalent ⟨111⟩ gaps induced by the stress. Stress-induced changes in $m^*$ are neglected because they give a less dispersive contribution to the piezobirefringence than the changes in gap and matrix element. For the purpose of a fit to the experimental data this contribution can be considered to be included in the weakly dispersive contribution due to the $E_2$ gap to be discussed later. For a [100] stress the ⟨111⟩ gaps remain equivalent. Thus only changes in matrix elements due to a stress-induced coupling between the spin-orbit split valence bands contribute to the piezobirefringence. Following Ref. 19 we find

$$\left(\frac{\epsilon_\parallel-\epsilon_\perp}{X}\right)^{[001]}_{E_1,E_1+\Delta_1}=+\frac{16\sqrt{2}}{3}\frac{D_3^3(S_{11}-S_{12})}{a_0\Delta_1\omega_1}\times\left[-\frac{1}{x_1^2}\ln(1-x_1^2)+\left(\frac{\omega_1}{\omega_{1s}}\right)\frac{1}{x_{1s}^2}\ln(1-x_{1s}^2)\right]. \quad (13)$$

Equation (13) is identical to Eq. (91′) of Ref. 19 except for the correction of two misprints and for having expressed $\delta\omega_1$ in terms of the deformation potential $D_3^3$ as given in Ref. 20,

$$\delta\omega_1=(2\sqrt{2}/\sqrt{3})D_3^3(S_{11}-S_{12})X. \quad (14)$$

For a [111] stress both energy splittings of the ⟨111⟩ gaps and matrix element changes contribute to the piezobirefringence. The net effect is given by [see Eq. (96) of Ref. 19]

$$\left(\frac{\epsilon_\parallel-\epsilon_\perp}{X}\right)^{[111]}_{E_1,E_1+\Delta_1}=\frac{16\sqrt{2}}{9}\frac{S_{44}D_3^5}{a_0\omega_1\Delta_1}\left[-\frac{1}{x_1^2}\ln(1-x_1^2)+\left(\frac{\omega_1}{\omega_{1s}}\right)\frac{1}{x_{1s}^2}\ln(1-x_{1s}^2)\right]+\frac{8}{9}\frac{D_1^5S_{44}}{a_0\omega_1^2}\left[\frac{1}{1-x_1^2}+\left(\frac{\omega_1}{\omega_{1s}}\right)^2\frac{1}{1-x_{1s}^2}\right]. \quad (15)$$

Throughout this work the *compressive* stresses applied in our experiments are assumed to be *negative*. The first term in the right-hand side of Eq. (15), analogous to Eq. (13), is due to changes in matrix elements produced by the stress-induced intravalence band splitting $\delta\omega_1$ of Ref. 19 expressed in terms of the deformation potential[20] $D_3^5$

$$\delta\omega_1=\tfrac{1}{2}\sqrt{\tfrac{2}{3}}D_3^5S_{44}X. \quad (16)$$

The second term on the right-hand side of Eq. (15) represents the effect of the stress-induced splittings of the ⟨111⟩ gaps. The deformation potential $\mathcal{E}_2$ of Ref. 19 has been expressed in terms of $D_1^5$ of Ref. 20.

$$\mathcal{E}_2=(\sqrt{3}/2)D_1^5. \quad (17)$$

Although the second term in Eq. (15) is in principle more dispersive than the first one, in the limit of small spin-orbit splitting (a condition that holds in silicon since $\Delta_1=0.04$ eV and $\omega_1=3.3$ eV) the difference between the logarithmic terms also tends to a singularity of the type $(1-x_1^2)^{-1}$, plus another less dispersive term. We shall assume that these less dispersive terms are included in the contribution due to the $E_2$ gap and in this approximation we can write

$$\left(\frac{\epsilon_\parallel-\epsilon_\perp}{X}\right)^{[111]}_{E_1,E_1+\Delta_1}=\frac{8}{9}\frac{S_{44}}{a_0\omega_1^2}(D_1^5+2\sqrt{2}D_3^5)\times\left[\frac{1}{1-x_1^2}+\left(\frac{\omega_1}{\omega_{1s}}\right)^2\frac{1}{1-x_{1s}^2}\right]. \quad (18)$$

It is obvious from this expression that no information on the relative magnitudes of $D_1^5$ and $D_3^5$ can be obtained from a fit to the experimental results.

### B. Contribution from the $E_2$ gap

Owing to lack of information on the nature of the $E_2$ gap, contributions to piezobirefringence are approximated by a constant[19] or a harmonic oscillator dispersion.[1] We use the harmonic oscillator approximation to fit our data; however, the difference between using a harmonic oscillator and a constant is not found to be critical since the energy region of interest is sufficiently far from this gap, which is at 4.4 eV. The contribution to piezobirefringence from this gap is written as[1]

$$[(\epsilon_\parallel-\epsilon_\perp)/X]_{E_2}\sim 1+2x_2^2, \quad (19)$$

where $x_2=\omega/\omega_2$, and $\omega_2$ is the energy of the $E_2$ gap. Equation (19) was derived under the assumption of an effect due only to stress induced changes in the gap. If the effect is due mainly to changes in matrix elements, the factor of 2 in front of the $x_2^2$ term Eq. (19) would have to be removed. We have tried to use this factor as a fitting parameter without any significant improvement in the fits to experimental data. We therefore use a factor of 2 throughout the discussion.

The total contribution from both $E_1$, $E_1+\Delta_1$ and $E_2$ gaps for [001] stress therefore is

$$\left(\frac{\epsilon_{\parallel}-\epsilon_{\perp}}{X}\right)^{[001]} = +\frac{16\sqrt{2}}{3}\frac{D_3^3(S_{11}-S_{12})}{a_0\Delta_1\omega_1} \times\left[-\frac{1}{x_1^2}\ln(1-x_1^2) +\left(\frac{\omega_1}{\omega_{1s}}\right)\frac{1}{x_{1s}^2}\ln(1-x_{1s}^2)\right] + C_2(1+2x_2^2) \quad (20)$$

and for [111] stress

$$\left(\frac{\epsilon_{\parallel}-\epsilon_{\perp}}{X}\right)^{[111]} = \frac{8}{9}\frac{S_{44}}{a_0\omega_1^2}(D_1^5+2\sqrt{2}D_3^5) \times\left[\frac{1}{1-x_1^2}+\left(\frac{\omega_1}{\omega_{1s}}\right)^2\frac{1}{1-x_{1s}^2}\right] + C_2'(1+2x_2^2). \quad (21)$$

In Fig. 6 we plot the experimental points (triangles) obtained for $(\epsilon_{\parallel}-\epsilon_{\perp})/X$ with $\vec{X}\parallel[001]$. The points above 1.5 eV were obtained in this work and those below 1.5 eV from Ref. 1. Using Eq. (20), $\omega_1 = 3.3$ eV, $\omega_{1s} = 3.344$ eV, and $\omega_2 = 4.4$ eV, and using the elastic compliance constants of Ref. 21, we obtained the best fit for $D_3^3 = -1.8$ eV and $C_2 = 2.27\times10^{-11}$ cm$^2$/dyn (solid line). Previous measurements of $D_3^3$ indicate a value close to $-4$ eV.[18,22] For comparison, we plot the fit obtained for this value of $D_3^3$ with $C_2 = 2.8\times10^{-11}$ cm$^2$/dyn (Fig. 6, dashed lines). We also plot in Fig. 6 $(\epsilon_{\parallel}-\epsilon_{\perp})/X$ obtained from the Kramers-Kronig analysis[5] of the data of Ref. 4 (squares). Since only relative values as a function of energy are obtained in the work of Ref. 4 we have scaled the results to compare them with ours. The agreement between this data (after scaling), our experimental values and the fit for $D_3^3 = -1.8$ eV is good, particularly around the energy at which $(\epsilon_{\parallel}-\epsilon_{\perp})/X$ drops to zero (antiresonance), which is independent of the scaling of the results of Refs. 4 and 5.

In Fig. 7 we plot $(\epsilon_{\parallel}-\epsilon_{\perp})/X$ versus energy for [110] stress and a (001) scattering face. The circles indicate experimental points, those below 1.5 eV obtained from Ref. 1 and those above 1.5 eV from present experiments. (The filled circles are plotted on the scale marked in figure, the open circles on a 10× expanded scale.) The best fit of Eq. (21) to experiment, using $C_2'$ and $D_1^5+2\sqrt{2}D_3^5$ as adjustable parameters is indicated by the solid line, obtained for $C_2' = -1.3\times10^{-11}$ cm$^2$/dyn and $D_1^5+2\sqrt{2}D_3^5 = 40.6$ eV. The transition energies used were $\omega_1 = 3.3$ eV, $\omega_{1s} = 3.344$ eV, and $\omega_2 = 4.4$ eV. Though the fit is very good, the deformation potential $D_1^5+2\sqrt{2}D_3^5$ needed is about a factor of 2 larger than previously measured values.[18,22] Using the most favorable values from Ref. 18, $D_1^5+2\sqrt{2}D_3^5 = 22.3$ eV, (corresponding to $D_1^5 = 11$ eV and $D_3^5 = 4$ eV) we plot in Fig. 7 $(\epsilon_{\parallel}-\epsilon_{\perp})/X$ from Eq. (21) for $C_2' = 0$ (dashed lines). Agreement with experiment is seen to be worse. We also plot in Fig. 7 the scaled values obtained from Kramers-Kronig analysis of piezoreflectance data[4,5] (squares); they agree quite well with present experiments and the solid-line fit, as was the case for a [001] stress. The highest experimental point was obtained with our technique at $\omega = 3.38$ eV for a [110] stress, as indicated in Fig. 7. Due to the lack of points at intermediate frequencies we are not able to infer the sign of the effect at $\omega = 3.38$ eV. The theory is not expected to be sufficiently accurate at this frequency. In the frequency region close to the gap real transitions occur and the exact linewidth (not only the form of the singularity), including the imaginary part of the stress induced dielectric constant, is required for an accurate description. A second complication arises from the fact that the energy of the $E_1$ gap increases under uniaxial stress so that the energies of the incident and scattered light lie in the region of a singularity that is shifting as stress is applied. In fact, we observed a resonance enhancement of the intensity of the phonon as the gap reached the energy of the scattered radiation. As such, the measurement of $\pi_{44}$ at this energy is representative only of the approximate magnitude, and indicates the limit at which the present method can be used to measure the piezo-optical constants in silicon. The large experimental error in the result at 3.38 eV arises from the small change in the intensity ratio $\beta$ (Fig. 2) as a function of stress, which in turn is due to the small penetration depth.

As already mentioned, discrepancies of factors of 2 appear between previous determinations of $D_3^3$ and $D_1^5+2\sqrt{2}D_3^5$ and the present values obtained from our fits to $\pi_{11}-\pi_{12}$ and $\pi_{44}$. The previously determined values are higher than the present one for $D_3^3$ and lower for $D_1^5+2\sqrt{2}D_3^5$. This fact excludes the possibility of correcting the discrepancy by changing the oscillator strength of the $E_1$ transitions [Eqs. (12)]. The discrepancy may lie in the simplicity of our model, but it should also be noted that experimental determinations differ considerably among themselves.[22] Previous values were determined by tracking the frequency dependence of a rather broad reflectivity peak which may not adequately represent the critical energy $E_1$ which enters into Eqs. (12).

While our measurements alone do not allow us to determine the sign of $(\epsilon_{\parallel}-\epsilon_{\perp})/X$ and therefore those of the piezo-optical constants or deformation potentials, by extrapolating our results to long wavelengths so that they are compatible with

those of Higginbotham *et al.*,[1] we obtain $\epsilon_{\parallel} - \epsilon_{\perp}$ to be negative for compressive stresses ($X$ negative) along [001] and [111] at energies far from the gap, so that the piezo-optical constants $\pi_{11} - \pi_{12}$ and $\pi_{44}$ are negative [Eq. (11c)] in this region. Upon approaching the $E_1$ gap, $(\epsilon_{\parallel} - \epsilon_{\perp})/X$ for [001] stress (Fig. 6) approaches zero close to 3 eV and is expected to change sign and become negative [Eq. (20)] between 3 eV and the energy of the $E_1$ gap: in this region the dominant term in Eq. (20) is the one that contains $D_3^3$, so we conclude that $D_3^3$ is negative. By a similar argument, for $\vec{X} \parallel [111]$, $(\epsilon_{\parallel} - \epsilon_{\perp})/X$ remains positive from low energies up to the region below the $E_1$ gap (Fig. 7), so that $D_1^5 + 2\sqrt{2}\, D_3^5$ is positive. In order to obtain the best possible agreement between previous determinations of the deformation potentials[22] and the present ones, we conclude that both $D_1^5$ and $D_3^5$ must have the same sign, i.e., positive. Earlier work[18,22] yielded only the magnitudes of $D_3^5$ and $D_3^3$ but not their signs. The sign of $D_1^5$ can, however, be inferred from Refs. 18 and 22 to be positive as well. A positive sign for $D_1^5$ has also been found for Ge, GaAs,[23] GaSb, and InSb.[24]

## V. CONCLUSIONS

Two combinations of piezo-optical constants of silicon have been measured as a function of photon energy in the region 1.65–3.4 eV where the material is opaque. A technique based on the depolariztion of Raman structures upon application of uniaxial stress was used. We found the magnitude of the piezo-optical constant $\pi_{11} - \pi_{12}$ to decrease with increasing frequency reversing sign (antiresonance) at about 3.0 eV, while that of $\pi_{44}$ was found to increase strongly without reversing sign. This dispersion of piezobirefringence was fitted with a theory based on a two-dimensional critical point model of the $E_1$ gap.

From this fit the sign and magnitude of three deformation potentials related to the $E_1$ gap were determined. They agree to within a factor of 2 with determinations based on different experimental techniques.

*Note added in proof.* Contrary to the statements made in the text, it has been found that the sign of the elasto-optical constants can be determined by inserting a Babinet compensator in the incident beam and determining if it enhances or decreases the observed depolarization of the scattered light. If the fast and slow axes of the compensator are known, the sign of the $\pi_{ij}$ can be deduced.

## ACKNOWLEDGMENT

One of us (M. H. G.) was supported by the Alexander von Humboldt Foundation.

[1] C. W. Higginbotham, M. Cardona, and F. H. Pollak, Phys. Rev. 184, 821 (1969), and references therein.
[2] P. Y. Yu, M. Cardona, and F. H. Pollak, Phys. Rev. B 3, 340 (1971); A. Yu Shileika, M. Cardona, and F. H. Pollak, Solid State Commun. 7, 1113 (1969); A. Gavini and M. Cardona, Phys. Rev. 177, 1351 (1969).
[3] R. W. Dixon and M. G. Cohen, Appl. Phys. Lett. 8, 205 (1966).
[4] G. W. Gobeli and E. O. Kane. Phys. Rev. Lett. 15, 142 (1965).
[5] M. Cardona, *Modulation Spectroscopy* (Academic, New York, 1969), p. 152.
[6] M. Chandrasekhar, M. H. Grimsditch, and M. Cardona, J. Opt. Soc. Am. 68, 523 (1978).
[7] H. Vogelmann and T. A. Fjeldly, Rev. Sci. Instrum. 45, 309 (1974).
[8] Trademark, Monsanto Corporation.
[9] D. F. Nelson, P. D. Lazay, and M. Lax, Phys. Rev. B 6, 3109 (1972).
[10] J. F. Nye, *Physical Properties of Crystals* (Clarendon, Oxford, 1960), p. 253.
[11] R. Loudon, Adv. Phys. 13, 423 (1964).
[12] M. Chandrasekhar, J. B. Renucci, and M. Cardona, Phys. Rev. B 17, 1623 (1978).
[13] P. A. Temple and C. E. Hathaway, Phys. Rev. B 7, 3685 (1973).
[14] H. R. Philipp, J. Appl. Phys. 43, 2835 (1972); and private communication.
[15] E. O. Kane, Phys. Rev. 146, 558 (1966).
[16] D. Brust, Phys. Rev. 134, A1337 (1964).
[17] M. Cardona and F. H. Pollak, Phys. Rev. 142, 530 (1966).
[18] F. H. Pollak and G. W. Rubloff, Phys. Rev. Lett. 29, 789 (1972), and references therein.
[19] M. Cardona, in *Atomic Structure and Properties of Solids*, edited by E. Burstein (Academic, New York, 1972), p. 514.
[20] E. O. Kane, Phys. Rev. 178, 1368 (1969).
[21] J. J. Hall, Phys. Rev. 161, 756 (1967).
[22] K. Kondo and A. Moritani, Phys. Rev. B 14, 1577 (1976).
[23] M. Chandrasekhar and F. H. Pollak, Phys. Rev. B 15, 2127 (1977), and references therein; Reference 5, p. 293.
[24] T. Tuomi, M. Cardona, and F. H. Pollak, Phys. Status Solidi 40, 227 (1970).